catalysts

MDPI

Article

Ternary Hydrotalcites in the Multicomponent Synthesis of 4*H*-Pyrans

Eliana Nope [1], Ángel G. Sathicq [1], José J. Martínez [2], Hugo A. Rojas [2], Rafael Luque [3,*] and Gustavo P. Romanelli [1,4,*]

1 Centro de Investigación y Desarrollo en Ciencias Aplicadas "Dr. Jorge J. Ronco" CINDECA—Facultad de Ciencias Exactas—Universidad Nacional de La Plata, 47 N° 257, La Plata 1900, Argentina; elianronova@gmail.com (E.N.); agsathicq@yahoo.com.ar (Á.G.S.)

2 Escuela de Ciencias Químicas, Facultad de Ciencias, Universidad Pedagógica y Tecnológica de Colombia UPTC, Avenida Central del Norte, Tunja, Boyacá 150003, Colombia; jose.martinez@uptc.edu.co (J.J.M.); hugo.rojas@uptc.edu.co (H.A.R.)

3 Departamento de Química Orgánica, Universidad de Córdoba, Campus de Rabanales, Edificio Marie Curie (C-3), Ctra Nnal IV-A, Km 396, E14014 Córdoba, Spain

4 CISAV, Cátedra de Química Orgánica, Facultad de Ciencias Agrarias y Forestales, Universidad Nacional de La Plata, Calles 60 y 119 s/n, La Plata B1904AAN, Argentina

* Correspondence: q62alsor@uco.es (R.L.); gpr@quimica.unlp.edu.ar (G.P.R.)

Received: 11 December 2019; Accepted: 30 December 2019; Published: 3 January 2020

Abstract: Lamellar double hydroxides (LDH) with double divalent cations were synthesized by the co-precipitation method and studied in the multicomponent synthesis of 4H-pyrans. The solids obtained were characterized by X-ray diffraction (XRD), infrared spectroscopy (FTIR), N_2 adsorption isotherms, and thermogravimetric analysis (TGA). The XRD patterns confirmed the formation of LDHs in which the incorporation of Ni^{2+} or Co^{2+} improves their crystalline and textural properties. The results of catalytic activity showed that the synthesis of 4*H*-pyrans is favored in solvent-free conditions with the LDH–Ni catalyst, avoiding calcination processes. In addition, it was found that hydrotalcite with double divalent cations can conduct this reaction through multicomponent synthesis or by the Michael addition reaction, which can be performed by different types of basicity that depend on the composition of another divalent cation in the brucite layer or a calcination process.

Keywords: hydrotalcites; 4*H*-pyrans; solvent-free; multicomponent reaction

1. Introduction

Hydrotalcites are materials known as lamellar double hydroxides (LDH) that have divalent (Me^{2+}) and trivalent cations (Me^{3+}), which are generally described as $[Me^{2+}_{(1-x)}\,Me^{3+}_{x}(OH)^2]^{x+}\,(A^{n-})_{x/n}\bullet nH_2O$. Their structure presents brucite-type $Mg(OH)_2$ layers, where the isomorphic substitution of Mg^{2+} by Al^{3+} or by cations with similar ionic radius results in positive net charge compensated by interlaminar anions (A^{n-}) and crystallization water [1]. These materials have high adsorption capacity, functionalization, and great chemical and thermal stability, and due to their acid–base properties, they have been widely used in chemical synthesis.

The adjustment of the acidic or basic properties of LDHs or mixed oxides that are generated by calcination at high temperatures has recently been studied. However, it is known that the properties of LDHs can be adjusted through the modification of the ratio of metal cations [2] by calcination and reconstruction processes (memory effect) [3] or by the incorporation of another di- or trivalent cation in the brucite layer [4]. The possibility of modifying the cations or their ratio and the interlaminar anion makes these materials a very versatile system with desirable catalytic properties. Therefore, they are

promising precursors of various processes with wide applications, such as hydrogenation reactions, oxidation, addition, dehydration, condensation, and multicomponent reactions, among others.

A new approach in organic chemistry is the use of multicomponent reactions (MCRs). These reactions combine at least three reagents to generate a compound that contains most of the atoms of the starting materials, which usually result in heterocyclic compounds with high biological activity [5,6]. MCRs have proven to be a tool for the formation of strong and efficient bonds in organic, medical chemistry and in the context of green chemistry. Several investigations using hydrotalcites as heterogeneous catalysts have been reported in the field of MCRs [4,7–9]. It has been found that the ratio and type of metal cations, as well as the formation of mixed oxides (LDO) by calcination processes, are useful parameters for obtaining highly selective products. In this way, Kshirsagar et al. found that the catalytic activity of LDO is greater than that of LDH with an Mg/Al ratio = 5, for the single-step synthesis of functionalized cyclohexenes [7]. In other investigations, it was found that a ratio of Mg/Al = 3 leads to the formation of 2-aminochromenos [8], while a ratio of Mg/Al = 2 favors the synthesis of dihydropyridines. In addition, the incorporation of V^{2+} and Zn^{2+} improves the catalytic performance, but when Co^{2+} or Ni^{2+} is incorporated, it decreases [4]. The synthesis of dihydropyran-chromenes is favored by the replacement of Cu^{2+} in the brucite layer [9].

2-amino-4*H*-pyran compounds have a structure of significant importance since they are found in several natural products, have pharmacological activity, and exhibit anticancer [10], antifungal, antimicrobial, and anti-inflammatory properties [11–13]. Given this broad spectrum of biological activity, several methodologies have been studied for their synthesis. The synthesis to obtain 4*H*-pyrans involves an MCR that includes a Knoevenagel condensation between the aldehyde group and the active methylene compound. The formed intermediate reacts by Michael addition with the β-dicarbonyl compound, and finally with the closure of the ring, the 4*H*-pyran compound is obtained (Scheme 1), this reaction generally involves the use of conventional basic catalysts that hinder the extraction and purification processes [13].

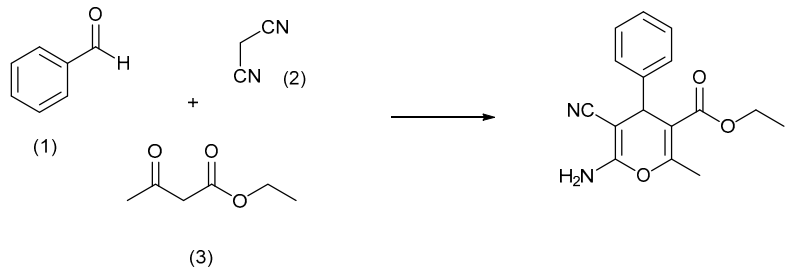

Scheme 1. Multicomponent reaction of 4*H*-pyrans. Benzaldehyde (1), malononitrile (2), and ethyl acetoacetate (3).

Several heterogeneous catalysts have been studied in the synthesis of 4*H*-pyrans. It has been reported that the reaction is favored by the modification of basic properties by calcination processes, so LDHs with Mg/Al ratios = 2, 3, and 5 were calcined at 773 K. The number of basic sites gradually increases with the Mg/Al ratio, obtaining yields of 80% when ethanol is used as the reaction solvent [14]. Dabholkar et al. also found similar results with Mg/Fe calcined at 773 K, where the elimination of hydration water molecules leads to the formation of metal oxides such as $MgFe_2O_4$ and MgO that favor the reaction with yields of 85% [15]. Mg/La LDH presented a strong basic character due to the formation of La_2O_3, reaching yields of 92%. Although high yields toward 4*H*-pyran are obtained, hydrotalcite requires high calcination temperatures, since the formation of mixed oxides favors the basicity required in the reaction, and the process leads to greater energy consumption [15]. However, as mentioned above, the properties of LDHs can also be changed with the incorporation of another divalent cation in the brucite layer.

Metals such as Cu^{2+}, Ni^{2+}, Fe^{2+}, Ca^{2+}, Co^{2+}, and Zn^{2+}, among others, can be incorporated into the laminar structure, which allows obtaining a great variety of materials with the catalytic properties

that are characteristic of each metal. However, it has been shown that Ni and Co favor the breakdown of C–C and O–H bonds and allow the generation of C–O bonds [16]. Therefore, catalytic systems that present double divalent cations in the brucite layer have been extensively studied in processes involving carbon desulfurization [17] in methane reforming reactions from CO_2 [18], the partial oxidation of methane or light paraffins [19], and the oxidative dehydrogenation of hydrocarbons, among others, but they have not been studied in multicomponent reactions. Due to their broad spectrum in terms of composition, they are very promising materials to carry out a one-pot synthesis. In this work, we studied the synthesis of hydrotalcites with double divalent cations in the multicomponent reaction of 4*H*-pyrans to avoid the calcination processes. We found that hydrotalcite with double divalent cations can conduct the reaction via multicomponent synthesis or directly by Michael addition reaction.

2. Results and Discussion

2.1. Catalyst Characterization

XRD patterns of the synthesized solids are presented in Figure 1. All samples exhibit diffraction patterns that are characteristic of hydrotalcite-type multilayer materials (JCPDS 00-014-0191). Furthermore, it is observed that LDH–Ni and LDH–Co present better crystallinity, which indicates that the incorporation of another divalent cation in the brucite layer gives greater crystallinity to LDH–Mg. In general, hydrotalcites consist of two-dimensional sheets of $Mg(OH)_2$-type brucite, so the divalent cation is sixfold coordinated to the OH– groups forming octahedrons that share their edges with other cations, creating sheets that are ordered one over another and are connected together via hydrogen bridge-type interactions. Thus, when a partial or total replacement of Mg^{2+} with another divalent cation of similar ionic radius occurs, the composition of the hydrotalcite can be described as $[MgM_{1-x}AlM_x(OH)_2]^{x+}$ [20,21].

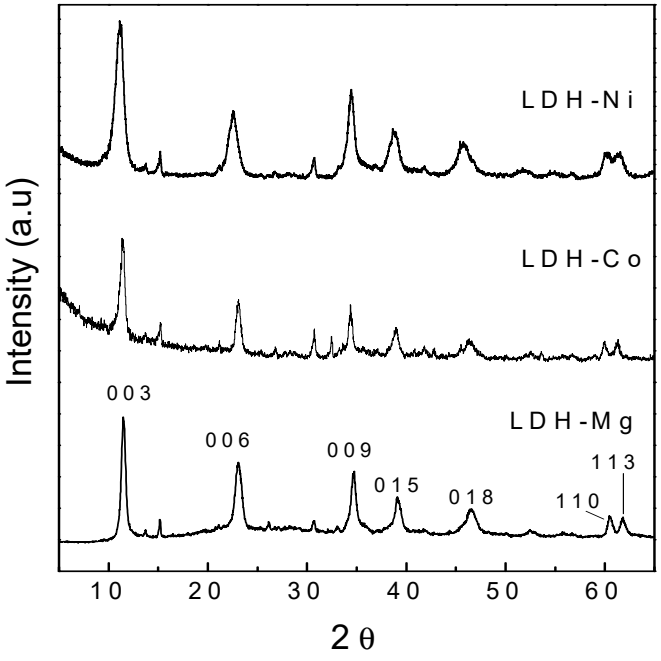

Figure 1. XRD patterns of the lamellar double hydroxides (LDHs).

In this case, reflections at low 2θ angles corresponding to (003) and (006) planes indicate the isomorphic substitution of Mg^{2+} for Ni^{2+} or Co^{2+} in the brucite layer [22,23]. However, other crystalline phases are observed in LDH–Co, which could indicate that small amounts of cobalt hydroxide (JCPDS 01-074-1057) were formed during the precipitation process. These results were also found by Qianhe Liu et al. for the ZnAlZr hydrotalcite [24].

On the other hand, the reflections at high 2θ angles with (110) and (113) planes indicate an adequate distribution of the anions in the intermediate layer and of the cations in the sheet layer [25]. The unitary cell parameters *a* and *c* calculated from the XRD results in Table 1 show that there is no significant change in the LDH–Mg with the incorporation of another divalent cation, and the hydrotalcite structure is maintained. Thus, the parameter a, which indicates the distance between the cations, is kept constant in the three materials. However, the parameter *c*, which is indicative of the layer size and the distance between layers, presents a slight change with the incorporation of nickel or cobalt.

Table 1. Lattice parameters of synthesized hydrotalcites.

Catalyst	Lattice Parameters		*d* (Å)
	a (Å)	*c* (Å)	
LDH	3.07	23.23	7.69
LDH–Ni	3.07	23.36	7.72
LDH–Co	3.07	23.43	7.78

The parameter *c* depends on the size of the cation, the charge density, and the nature of the anion in terms of size, quantity, and orientation, and may also be indicative of the amount of water molecules present in the interlaminar space [26]. The value of this parameter in the synthesized materials is around 23–24 Å, which is typical of carbonate anions, although NO^{3-} anions could also be present [22]. The slight change in the parameter c can be associated with the results of the interplanar distance calculated from the reflection (003) shown in Table 1. It can be observed that this value increases in LDH–Ni and LDH–Co, and could be related to the incorporation of another divalent cation in the laminar structure. So, the substitution of nickel or cobalt in brucite provides a larger number of CO_3^{2-} anions in the interlaminar layer in order to neutralize the excess positive charges. Consequently, the distance between the layers and the parameter c increase [24]. It should be noted that the increase of these parameters in LDH–Co could also be related to small amounts of cobalt hydroxide in the laminar structure.

Textural properties of the synthesized hydrotalcites are summarized in Table 2, which shows that the incorporation of Ni^{2+} and Co^{2+} in the structure of LDH–Mg increased the surface area value. So, it is observed that LDH–Ni has the greatest surface area, which could indicate that nickel has greater stability in the laminar structure than cobalt [22,27,28]. In addition, a change in the pore volume is observed, being more predominant in LDH–Ni. On the other hand, the change in the textural properties in LDH–Mg can also be related to the increase of the carbonates in the interlaminar space, due to the addition of another divalent cation in the brucite layer, as described in the XRD results.

Table 2. Textural and basic properties determined by titration with 0.01 M benzoic acid.

Catalyst	S_{BET} ($m^2\ g^{-1}$)	Pore Volume ($cm^3\ g^{-1}$)	Pore Size (nm)	Basicity [a] (mmol/g)
LDH–Mg	17	0.11	8	0.016
LDH–Ni	42	0.21	9	0.321
LDH–Co	28	0.13	8.5	0.163

[a] 0.05 g hydrotalcite suspended in 2 mL of phenolphthalein solution is titrated with 0.01 M benzoic acid.

The pore size distribution curves inserted in Figure 2, which were calculated according to the Barrett, Joyner, and Halenda (BJH) method, show a unimodal distribution and are within the range of mesoporous materials [29], with values between 8 and 9 nm for the three materials. Although there is no significant change in the pore diameter value, it is observed that the modification of LDH–Mg with cobalt and nickel causes an increase in the pore density. In general, the textural properties of LDH–Mg

change with the introduction of another divalent cation. The change of the pore characteristics could be related to the isomorphic substitution of two divalent cations within the laminar structure, which causes an alteration of the microscopic morphology [30].

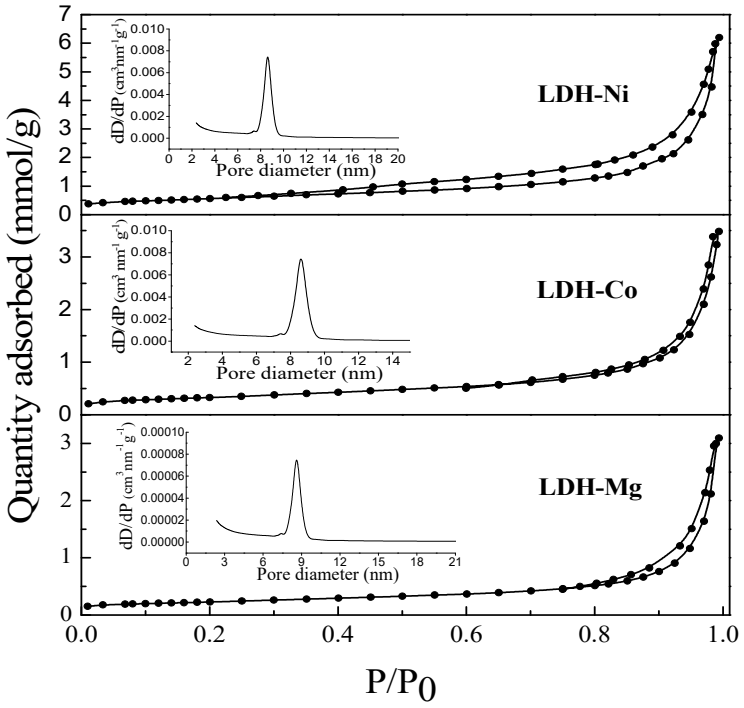

Figure 2. Adsorption–desorption isotherms at 77 K and pore size distribution of synthesized LDH.

The adsorption–desorption isotherms of these materials are presented in Figure 2. It can be seen the solids present type IV isotherms that are characteristic of mesoporous materials with an H3 hysteresis loop [31]. This type of loop indicates the formation of plate-like materials, where the pores of the particles are slit-like, which is characteristic of hydrotalcite-type materials [29].

The infrared spectrum of the solids obtained is shown in Figure 3. All materials show characteristic hydrotalcite-type bands. A predominant band between 3400 and 3700 cm^{-1} corresponds to –OH stretching vibrations of the hydroxyl groups and water molecules found in the interlaminar region, while a bending band at 1639 cm^{-1} is assigned to the water molecules present between the layers [25,32]. The band at 1384 cm^{-1} is attributed to the antisymmetric stretching mode of carbonate anion in the interlaminar layer, while other bands at 625 and 823 cm^{-1} are related to vibrational modes of CO_3^{2-} [1,33]. This indicates that the carbonate ion is found as free anions that balance the positive charge of the lamellar layers and confirms the formation of carbonate ions in the hydrotalcite structure [34]. In addition, it can be observed that the carbonate ion bands are more predominant in LDH–Ni and LDH–Co. The band between 2500 and 3000 cm^{-1} is attributed to the hydrogen bond between H_2O and carbonates in the interlaminar layer [35]. This band, which is only observed for LDH–Ni, indicates that the substitution of nickel in the brucite layer could increase the basic properties of this material.

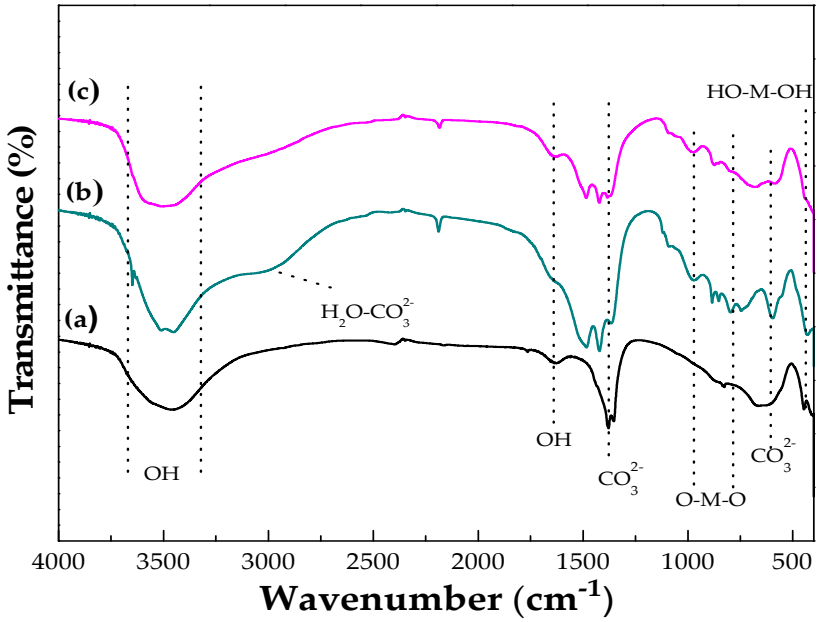

Figure 3. The infrared spectrum of the LDH, (**a**) LDH–Mg, (**b**) LDH–Ni, and (**c**) LDH–Co.

Some vibrations in the 400 to 1000 cm^{-1} region could be related to oxygen–metal vibrations in the brucite layer; the bands around 400 and 550 cm^{-1} are assigned to vibrational modes δHO–M–OH and δO–MO (M = metal) [36]. Furthermore, the band between 3400 and 3700 cm^{-1} of the LDH–Mg solid moves to higher frequencies in LDH–Ni and LDH–Co, which could indicate a change in the bond strength of M–OH due to the presence of another metal in the hydrotalcite structure [37]. New bands in the 700 to 1000 cm^{-1} region are observed in the spectra of LDH–Ni and LDH–Co, possibly indicating the formation of M–OH bonds [25].

The thermal decomposition of hydrotalcite-type materials generally has several stages of decomposition, which is why three temperature ranges are distinguished in which processes of dehydration, dehydroxylation, decarboxylation, and others occur [31]. The results of the thermogravimetric analysis of the synthesized materials are shown in Figure 4. A mass loss between 323 and 523 K can be observed, which is attributed to water molecules physically adsorbed on the surface and to water molecules adsorbed between the layers [3,38]. A mass loss of 10% is observed for LDH–Ni, 7% for LDH–Co, and 12% for LDH–Mg. However, in LDH–Ni, the first mass loss reaches 573 K, indicating that not only the loss of water molecules occurs but also the decomposition of the hydroxyl groups that are coordinated to the metal cations [26,39].

The dehydroxylation process for LDH–Co is evidenced between 473 and 623 K with a mass loss of 13%, although it could also be related to the small amounts of $Co(OH)_2$ that could be formed in the synthesis of this material, according to XRD results. For LDH–Mg, dehydroxylation extends up to 723 K with a mass loss of 12%, which indicates that the decomposition of OH groups and carbonate anions in LDH–Mg occurs simultaneously. The initial stage of decarboxylation in LDH–Ni and LDH–Co is observed between 573 and 673 K. The third mass loss is evidenced at temperatures above 673 K at which the total decomposition of carbonate anions and the formation of mixed oxides occur [35]. However, a slight mass loss at 723 K in the cobalt materials and nickel is attributed to the decomposition of possible nitrate anion species [40].

Although the three materials were synthesized under the same synthesis parameters, it is observed that only with the incorporation of a second divalent cation, the properties of LDH–Mg are modified and different thermal stabilities are generated. This stability depends mainly on the type of cation incorporated, which could confer better properties in catalytic activity studies.

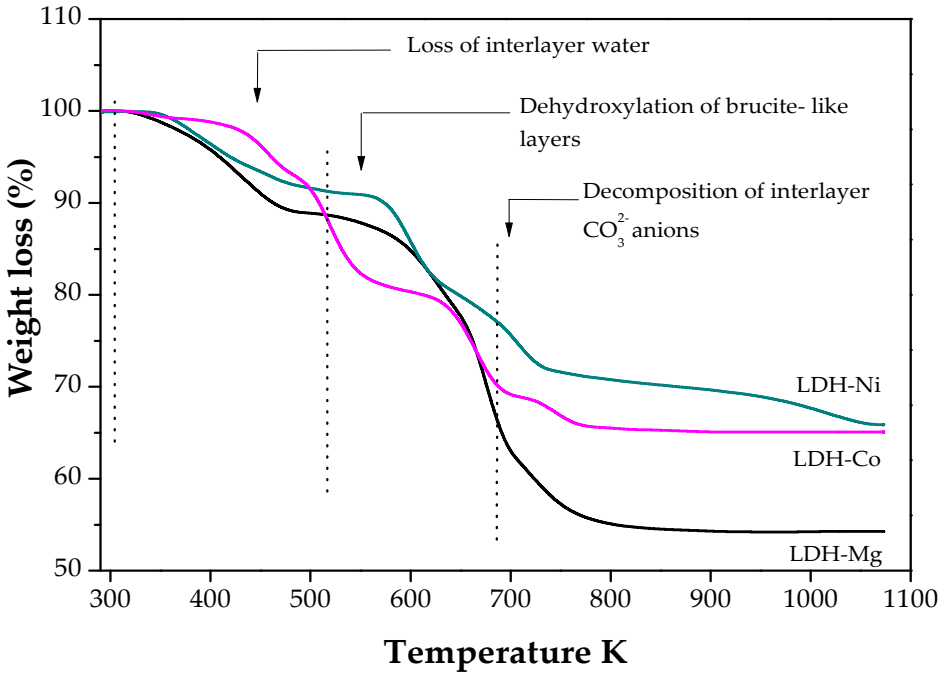

Figure 4. Thermogravimetric analysis of LDH.

When Ni^{2+} replaces the Mg^{2+} sites, the Ni^{2+} species are highly dispersed [28]. This dispersion could improve the basic properties of this material. Although the temperature-programmed analysis of CO_2 desorption is a method that allows measuring the basicity, in the case of hydrotalcite-type materials, this analysis could destroy the structure of these materials since high temperatures are required to perform it. So, in this work, the basic properties of the synthesized materials were determined by titration with 0.01 M benzoic acid. The results in Table 2 show that the incorporation of a second divalent cation in the hydrotalcite increases the number of basic sites, being more predominant in LDH–Ni, which is possibly related to the increase of the carbonate anions in the interlaminar layer, given that the basic sites in hydrotalcites are generated by the OH^- and HCO_3^- species [20]. This result indicates that the performance of the reaction is favored by the increase of basic sites in LDH–Ni.

2.2. Catalytic Activity

For the catalytic activity studies, a mixture of benzaldehyde (1), malononitrile (2), and ethyl acetoacetate (3) (Scheme 1) was used as a test reaction. To optimize the reaction conditions, the effect of the solvent was initially evaluated using LDH–Mg at room temperature. The results in Table 3 show that the reaction is favored in solvent-free conditions with yields of 30% toward 4*H*-pyran. These findings indicate that probably the absence of solvent allows a better interaction of the reagents with the catalyst [41–43]. Although the synthesis of 4*H*-pyrans has been reported in solvents such as ethanol, methanol, and water among others [44], solvent-free reactions are an alternative for the reduction of residual solvents; they have low cost, simplicity in reactions, and high process selectivity. The reaction was studied in different polar solvents, and although the final product is obtained, 48 h are required for its formation, and only 30% conversions are achieved.

Table 3. Effect of the solvent.

Solvent	Yield to 4*H*-Pyran (%)	Time (h)
Water	21	48
Ethanol	25	48
Ethyl acetate	27	48
Solvent-free	30	8

Reaction conditions: Benzaldehyde (1 mmol), ethyl acetoacetate (1 mmol), malononitrile (1 mmol), LDH–Mg catalyst (30 mg), solvent: 30 mL, room temperature.

To evaluate the effect of the metal on the reaction, LDH–Ni and LDH–Co were tested. Initially, the reaction temperature was studied under solvent-free conditions for 8 h of reaction. In Table 4, it can be seen that the reaction shows better yields with LDH–Ni at 353 K. This result can be related to the basic, textural, and structural properties of LDH–Ni. As mentioned above, the isomorphic substitution of another divalent cation in the brucite layer can modify the hydrotalcite properties; so, the substitution of Mg^{2+} for Ni^{2+} gives it greater surface area, greater basicity, and better thermal stability. This is related mainly to the increase of the interlaminar anion, the HCO_3^- and OH^- species being the ones that provide the basic sites and those that possibly lead to the formation of 4*H*-pyran.

Table 4. Effect of the metal.

Catalyst	Yield (%)			
	Room Temperature		353 K	
	Intermediate	4*H*-Pyran	Intermediate	4*H*-Pyran
LDH–Mg	40	23	43	34
LDH–Ni	28	39	20	58
LDH–Co	25	28	18	40

Reaction conditions: benzaldehyde (1 mmol), ethyl acetoacetate (1 mmol), malononitrile (1 mmol), catalyst (30 mg); 8 h, solvent-free, and 300 rpm agitation.

As the reaction presented the best results with LDH–Ni, we decided to optimize the reaction conditions with this catalyst. The first parameter to be evaluated was the optimal amount of catalyst for the reaction. The results at 8 h of reaction are shown in Figure 5 and indicate that with less than 40 mg, the reaction is not selective to 4*H*-pyran, favoring the formation of the Knoevenagel intermediate and other unidentified products. However, it is observed that with amounts greater than 40 mg, the reaction is selective to 4*H*-pyran and yields greater than 80% are reached. These results reveal that the reaction is conducted through the product of Knoevenagel condensation between benzaldehyde and malononitrile. Therefore, greater amounts of catalyst or another type of basic force are required to convert this product into the 4*H*-pyran compound, taking into account that the determination of basicity was carried out with phenolphthalein, which is an indicator of strong basic sites. In addition, the titration was also carried out with bromothymol blue (an indicator of weak sites) but there was no change in the materials, so it could be affirmed that the reaction is carried out by the strong basic sites [45].

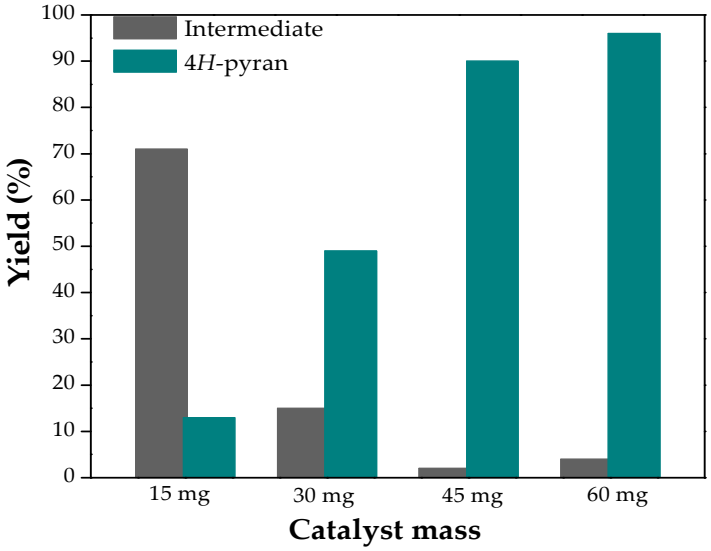

Figure 5. Effect of catalyst amount. Reaction conditions: benzaldehyde (1 mmol), ethyl acetoacetate (1 mmol), malononitrile (1 mmol), solvent-free, 8 h, 353 K.

Taking into account the possible mechanism of the reaction in which, after the Knoevenagel condensation, Michael 1,4-addition occurs, followed by the opening of the intramolecular ring (Scheme 2) [46], it could be affirmed that it is at this stage where the catalyst presents the greatest activity. Furthermore, the reaction without catalyst leads to the formation of the intermediate only, so that in the reaction, the basic character of the catalyst is necessary for the formation of 4*H*-pyran.

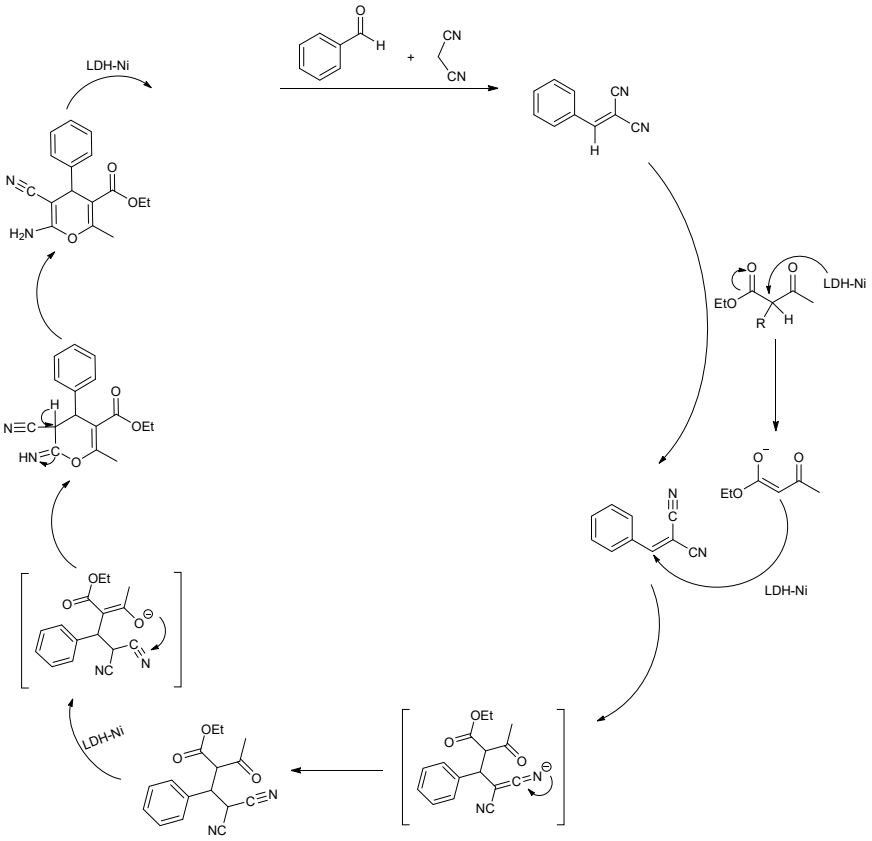

Scheme 2. 4*H*-pyrans reaction mechanism.

The effect of temperature on the reaction was evaluated using 45 mg of LDH–Ni. The results from Table 5 pointed to an increase in temperature favoring the selectivity toward 4*H*-pyran, with higher yields reached at temperatures above 333 K, 353 K being the optimum reaction temperature. This behavior could be related to the stage of Michael addition, since it has been shown that a change in the temperature of this reaction leads to the formation of other products. Thus, for example, it has been reported that in the Hantzsch reaction in the stage corresponding to the Michael 1,4 addition, the selectivity changes depending on the reaction temperature [47].

Table 5. Effect of temperature on the 4*H*-pyran reaction.

LDH–Ni	Selectivity (%)			
Temperature	**293 K**	**333 K**	**353 K**	**393 K**
Intermediate	30	7	2	6
4*H*-pyran	59	89	90	89

Reaction conditions: benzaldehyde (1 mmol), ethyl acetoacetate (1 mmol), malononitrile (1 mmol), catalyst (45 mg), 8 h, solvent-free, and 300 rpm agitation.

As mentioned above, the synthesis of 4*H*-pyran involves a multicomponent reaction in which two reactions are generated. First, there is a Knoevenagel condensation between benzaldehyde and malononitrile, forming an intermediate that then reacts with ethyl acetoacetate through a Michael 1,4 addition, which leads to the product 4*H*-pyran. In order to determine the reaction rate (k) and subsequently the activation energy (Ea) between 293 and 393 K and taking into account the results reported by Haas and Tallarek [48], in this reaction, we assume two orders of reaction, a pseudo first-order reaction for the reaction between benzaldehyde and malononitrile, where the formation of the intermediate occurs instantaneously even without a catalyst, and a second-order reaction for Michael addition, which is probably the predominant stage in the formation of 4*H*-pyran. In this way, the determination of the speed constants (k) was performed by plotting 1/[I] versus t, where [I] is the concentration of the intermediate formed in the reaction over time (t). It was observed that at room temperature, Michael addition is slower, and the reaction rate increases significantly at high temperatures. Therefore, the temperature favors this step. On the other hand, the apparent activation energy was calculated with the Arrhenius equation by means of a linear adjustment, which was determined by the graph of Ln (K) versus 1/T (T = temperature in Kelvin) obtaining a value of 22 KJ/mol for this step.

The hydrotalcites may have a bifunctional acid–base behavior, with the addition of different divalent cations or by calcination processes. To deduce whether the basic properties of this material are affected by calcination processes or by the incorporation of another divalent cation, the LDH–Ni material was calcined at 773 K (LDO–Ni) for 3 h using a heating rate of 273 K/min, and the reaction was monitored in order to study the time necessary to reach 100% conversion to the product of the reaction at 353 K.

The reaction was monitored using 45 mg of LDH–Ni and LDO–Ni under solvent-free conditions. Figure 6 clearly shows that the reaction proceeds via formation of the Knoevenagel intermediate, which is consumed to form 4*H*-pyran product (12 h reaction, 97% yield using LDH-Ni). In the case of LDO–Ni, no significant changes could be observed in yields toward 4*H*-pyran. So, this behavior can be related to the type of basicity present in hydrotalcites [15,49]. It is known that hydrotalcites have Lewis basic sites and Brönsted basic sites [50,51]. Nevertheless, when hydrotalcites undergo a calcination process, Lewis basic sites increase and Brönsted basic sites decrease. The reaction with LDH–Ni is mediated by basic Brönsted sites, and the reaction with LDO–Ni is mediated by Lewis basic sites [8].

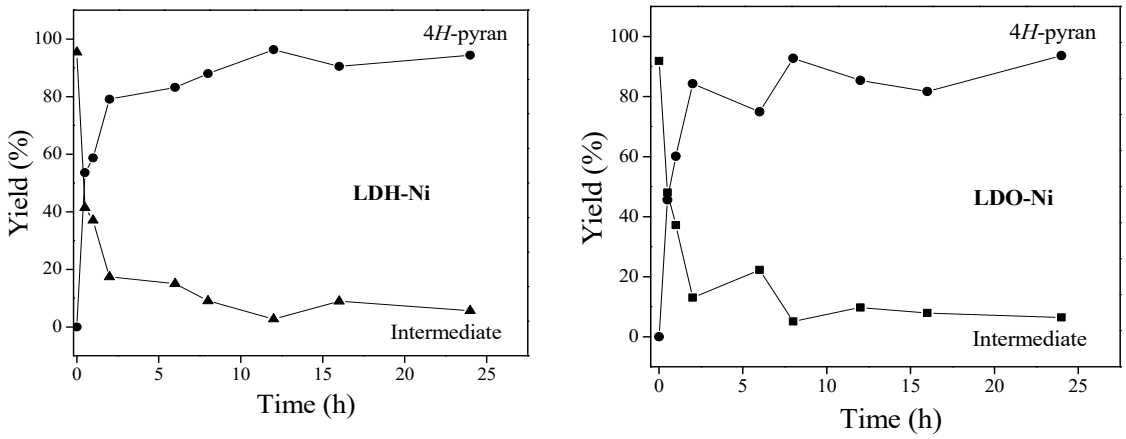

Figure 6. Reaction of 4*H*-pyrans with LDH–Ni and LDO–Ni.

In order to determine the basic character of LDH–Ni and LDO–Ni and to be able to assume the type of basicity that possibly leads the reaction, the temperature-programmed analysis of CO_2 desorption was carried out. Generally, hydrotalcite-type materials show three desorption peaks between 373 and 773 K that are associated with basic sites of weak, moderate, and strong character [52]. In Figure 7, it can be seen that the desorption profile for LDH–Ni shows three peaks that are associated with weak basic sites at 403 K, strong basic sites at temperatures >723 K, and a desorption peak above 973 K, which could be associated with the final stage of decarboxylation. This desorption peak is also observed in LDO–Ni. On the other hand, the moderate basic sites that occur in LDH–Ni are eliminated with the calcination process, and a desorption peak is observed at low temperatures, which could indicate a small contribution of weak basic sites. Peaks at low temperatures are attributed to basic Brönsted-type sites that are related to surface OH groups, and peaks at high temperatures can be attributed to basic Lewis-type sites due to the low coordination of oxygen atoms [53].

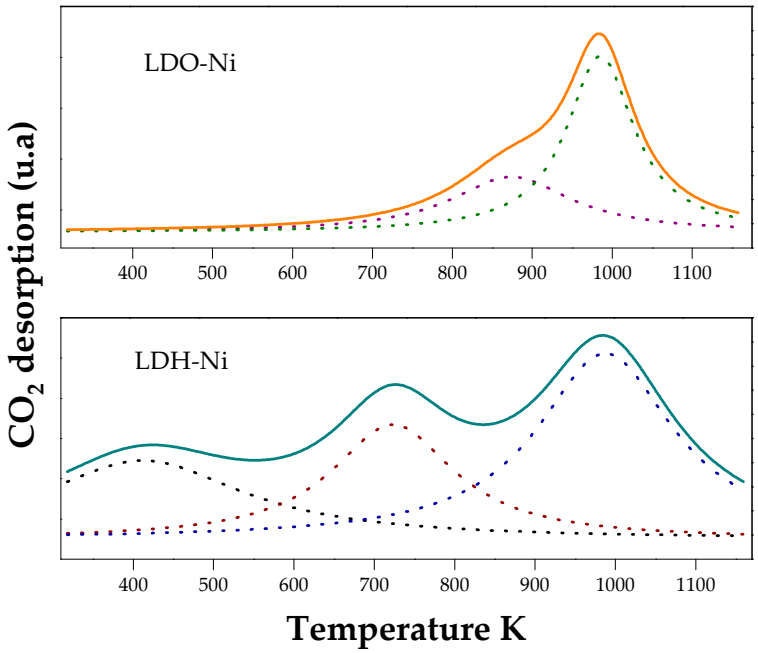

Figure 7. Analysis of CO_2 desorption of LDH–Ni and LDO–Ni.

Therefore, these results reveal that the reaction not only depends on the basicity, but also on the type of basic sites present in the catalyst. In this way, the reaction with LDO–Ni could be driven by the Lewis-type basicity that is generated at high temperatures. Although LDH–Ni presents weak and

moderate basic sites, it cannot be assured that these signals are related to the basicity of this material. As previously mentioned, they can be related to a possible decomposition of this material. However, there is a significant change with the calcination process, and possibly the basicity that drives the reaction is Brönsted type.

On the other hand, as we found that the catalyst LDH–Ni has greater activity in the Michael addition stage and that the reaction is conducted from the Knoevenagel intermediate, these results indicate that the reaction does not show a significant change in the yield toward 4*H*-pyran. Several investigations have demonstrated that the Michael addition reaction can be driven by different types of basicity. Thus, Choudary et al. [39] found that the hydrotalcite of rehydrated MgAl presents better yields compared to calcined and uncalcined hydrotalcite, since Brönsted-type basicity increases with the rehydration process. Hillary Prescott et al. [40] found an acid–base effect in calcined Mg/Al and similar yields in the addition of 2-methylcyclohexane-1,3-dione, 2-acetylcyclopentanone, and 2-acetylcyclohexanone to methyl vinyl ketone with calcined or uncalcined hydrotalcite. This behavior was also observed by Mohamed et al. [41] for MgAl hydrotalcite, calcined, and rehydrated, in the Michael addition reaction of enaminones with aminopyrazoles. These authors claimed that the Michael addition reaction depends on the acid and basic nature of the hydrotalcite, and that the location of the Al^{3+} cation in the cationic sheet is affected by calcination and rehydration processes. So, in the hydrotalcite, Al^{3+} cations play different roles, which together with the basic Brönsted sites act on the reaction.

We decided to study the synthesis of 4*H*-pyrans from the intermediate of the reaction, so we took 1 mmol of intermediate (previously synthesized and identified by NMR) and 1 mmol of ethyl acetoacetate using 45 mg of LDH–Ni at 353 K. The reaction was monitored for 24 h. In Figure 8, it can be seen that there is no significant change between the multicomponent reaction and the reaction from the Knoevenagel intermediate; only MCR shows better stability and similar performances are observed.

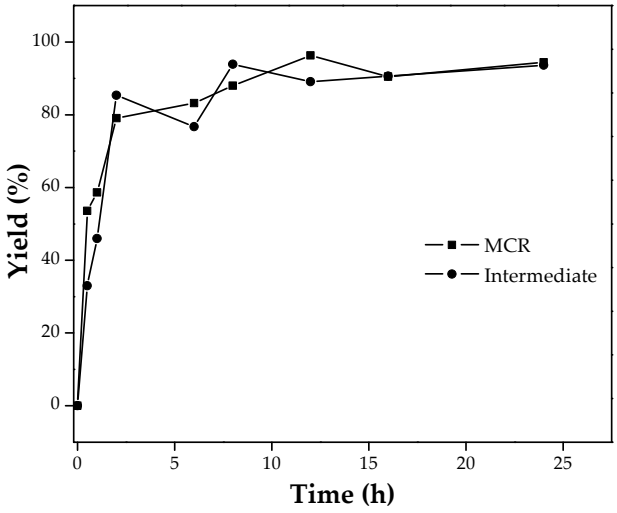

Figure 8. 4*H*-pyran synthesis via MCR and Michael addition with LDH–Ni.

In this way, the synthesis of 4*H*-pyran compounds can be conducted by different types of basicity that depend mainly on the composition of the divalent cations and the calcination processes. In this case, LDH–Ni allows obtaining the 4*H*-pyran compound, demonstrating that the reaction is conducted by Brönsted-type basicity. However, when it is calcined at 773 K, the reaction is favored by Lewis-type basicity. Thus, this catalyst is efficient in multicomponent and Michael addition reactions.

2.3. Reusability

Hydrotalcites are heterogeneous catalysts and can easily be recovered from the reaction mixture. In this case, the catalyst was separated by filtration; then, it was washed with hot acetone (3 × 3 mL)

and dried at 353 K in order to evaluate its reuse in various reaction cycles. In Table 6, It can be seen that the yield toward 4*H*-pyran is maintained up to two reaction cycles and decreases by 10% with the third reaction cycle. This possibly relates to some type of poisoning by the product. Nevertheless, LDH–Ni can be applied in other multicomponent reactions and Michael addition reactions.

Table 6. Reusability study.

	Reaction	Cycle 1	Cycle 2	Cycle 3
Yield of 4*H*-pyran (%)	97	94	92	87
Yield of intermediate	3	6	8	13

3. Materials and Methods

3.1. Synthesis of Hydrotalcites

Hydrotalcite-type materials were synthesized by the co-precipitation method [54]. The salts of $Mg(NO_2)_3$ $6H_2O$ and $Al(NO_3)_3{\cdot}9H_2O$ were mixed with a molar ratio of $Mg^{2+}/Al^{3+} = 3$; then, an amount of urea (2.61 mol) was added to the aqueous solution under constant stirring at 333 K for 12 h, and the samples were hydrolyzed at 373 K for 10 h. Finally, a 2 M alkaline solution of NaOH and Na_2CO_3 was added slowly maintaining a pH = 10, and the mixture was kept in an aging process for 24 h at 413 K with constant agitation. The precipitate obtained was washed with deionized water and dried at 353 K for 12 h. The solid obtained is called LDH–Mg.

The incorporation of nickel or cobalt in LDH–Mg, $[Mg^{2+}{}_{1-x}Al^{3+}{}_x(OH)_2]^{x+}$ $(CO_3{}^{2-})^{x/n}{\cdot}nH_2O$, where a part of Mg^{2+} is substituted isomorphically by Ni^{2+} or Co^{2+} in the brucite layer, was carried out by the co-precipitation method previously described [54]. For this, $Ni(NO_2)_3{\cdot}6H_2O$ and $Co(NO_2)_3{\cdot}6H_2O$ were used as precursor salts with a $Me^{2+}/Al^{3+} = 3$ ratio. This substitution can be described as $[(MgNi)^{2+}{}_{1-x}$ $Al^{3+}{}_x(OH)_2]^{x+}$ and $[(MgCo)^{2+}{}_{1-x}$ $Al^{3+}{}_x(OH)_2]^{x+}$; the materials obtained are called LDH–Ni and LDH–Co.

3.2. Characterization of Hydrotalcite

The X-ray diffraction patterns were recorded in PANalytical X'Pert Pro equipment using Cu K radiation (L = 1.54056 Å), in the 2θ range of 10–90°, with a count time of 1 s and a step size of 0.05° s^{-1}. N_2 adsorption–desorption isotherms of the solids were measured at 77 K in Micromeritics ASAP 2020 equipment. Samples were previously degassed at 373 K under vacuum for 18 h. The Brunauer–Emmett–Teller (BET) isotherm and Barrett, Joyner, and Halenda (BJH) method were used to calculate the specific surface area and pore volume. Fourier-transform infrared (FTIR) spectra were recorded on a Nicolet iS50 spectrometer in the range of 4500–600 cm^{-1} using pressed KBr pellets. Thermogravimetric analysis (TGA) was carried out on a Setaram thermobalance. The samples were placed in an alumina crucible and heated using a heating ramp of 278 K/min up to 1073 K under N_2 flowing at 20 cm^3/min. The CO_2 temperature programmed desorption (CO_2–TPD) analyses were performed in a Micromeritics Autochem II 2920. Prior to the adsorption of CO_2, the samples were preheated at 673 K in helium flow (25 mL/min) for 1 h. Then, they were saturated with pure CO_2 (30 mL/min) at 393 K for 30 min and purged with helium (25 mL/min) for 1 h to remove all physically adsorbed molecules. Basicity was determined using volumetric titration with 0.01 M benzoic acid in toluene and phenolphthalein as the pH indicator. So, 0.05 g of the catalyst was suspend in 2 mL of the indicator solution [55]. The titration was conducted in triplicate.

3.3. Catalytic Studies

The catalytic activity of the obtained solids was evaluated in the synthesis of 4*H*-pyrans. Hence, a mixture of benzaldehyde (1 mmol), malononitrile (1 mmol), ethyl acetoacetate (1 mmol), and catalyst (30 mg) under solvent-free conditions was heated and stirred. The reaction was monitored by TLC (EtOAc:

petroleum ether = 1:3). The optimization parameters of the reaction were followed by high-performance liquid chromatography, using a C-18 column and acetonitrile:water as the mobile phase.

The retention times (min) of the products were 6.7 for the Knoevenagel intermediate at a wavelength of 284 nm and 7.5 for 4*H*-pyran at a wavelength of 254 nm. The calculation of the conversion (in Equation (1)) of reactants and the selectivity (in Equation (2)) of the obtained products was performed with the following equations. The yield was determined by multiplying the conversion by selectivity.

$$Conversion\ (\%) = \frac{initial\ concentration\ -\ final\ concentration}{initial\ concentracion} * 100 \quad (1)$$

$$Selectivity\ (\%) \frac{concentration\ of\ the\ desired\ product}{\sum\ concentration\ of\ the\ products\ obtained} * 100 \quad (2)$$

4. Conclusions

Hydrotalcite-type materials were synthesized with the incorporation of two divalent cations, and their catalytic activity was evaluated in the multicomponent synthesis of 4*H*-pyran compounds. The incorporation of a second divalent cation in LDH–Mg modifies the textural properties, improves the thermal stability, gives it greater crystallinity, and increases its basic properties. These modifications predominate with the addition of nickel, so this material presents better catalytic activity, demonstrating that the synthesis of 4*H*-pyran compounds using hydrotalcites with two different divalent cations is mainly driven by the Michael addition step and thus, the reaction can be favored with basic Brönsted-type sites or with basic Lewis-type sites when LDO–Ni is calcined at 773 K. In this way, the synthesis of 4*H*-pyran compounds in solvent-free conditions can be conducted by different types of basicity, which depend mainly on the composition of the divalent cations and the calcination processes. Thus, LDH–Ni proves to be an efficient catalyst in multicomponent and Michael addition reactions, and it can also be reused in three reaction cycles without significant loss of performance of the 4*H*-pyran compound. Therefore, this catalyst allows highly efficient processes.

Author Contributions: Conceptualization and Methodology, E.N., Á.G.S., and G.P.R.; methodology E.N.; Writing—Original Draft Preparation, E.N.; Writing—Review and Editing, E.N., J.J.M., Á.G.S. and G.P.R.; Supervision, G.P.R., Á.G.S., J.J.M., H.A.R., and R.L.; Project Administration, G.P.R.; Funding Acquisition, G.P.R. and Á.G.S. All authors have read and agreed to the published version of the manuscript.

Funding: This work was supported by CONICET—UNLP and ERANET-LAC-1.

Acknowledgments: Á.G.S. and G.P.R. are members of CONICET. This work is a collaboration with the Laboratorio de Catálisis of the Universidad Pedagógica y Tecnológica de Colombia (UPTC).

Conflicts of Interest: The authors declare no conflict of interest.

References

1. Chagas, L.H.; De Carvalho, G.S.G.; Do Carmo, W.R.; San Gil, R.A.S.; Chiaro, S.S.X.; Leitão, A.A.; Diniz, R.; De Sena, L.A.; Achete, C.A. MgCoAl and NiCoAl LDHs Synthesized by the Hydrothermal Urea Hydrolysis Method: Structural Characterization and Thermal Decomposition. *Mater. Res. Bull.* **2015**, *64*, 207–215. [CrossRef]
2. Nguyen, H.K.D.; Nguyen, T.D.; Vu, A.T.; Nguyen, T.T. Preparation of Acid–Base Bi-Functional Hydrotalcite Based Catalyst for Converting Vietnamese Coconut Oil to Green Hydrocarbons. *Chem. Pap.* **2017**, *71*, 961–970. [CrossRef]
3. Lee, G.; Kang, J.Y.; Yan, N.; Suh, Y.-W.; Jung, J.C. Simple Preparation Method for Mg–Al Hydrotalcites as Base Catalysts. *J. Mol. Catal. A Chem.* **2016**, *423*, 347–355. [CrossRef]
4. Pagadala, R.; Maddila, S.; Dasireddy, V.D.B.C.; Jonnalagadda, S.B. Zn-VCO3 Hydrotalcite: A Highly Efficient and Reusable Heterogeneous Catalyst for the Hantzsch Dihydropyridine Reaction. *Catal. Commun.* **2014**, *45*, 148–152. [CrossRef]

5. Kolb, J.; Beck, B.; Dömling, A. Simultaneous Assembly of the β-Lactam and Thiazole Moiety by a New Multicomponent Reaction. *Tetrahedron Lett.* **2002**, *43*, 6897–6901. [CrossRef]
6. Cioc, R.C.; Ruijter, E.; Orru, R.V.A. Multicomponent Reactions: Advanced Tools for Sustainable Organic Synthesis. *Green Chem.* **2014**, *16*, 2958–2975. [CrossRef]
7. Kshirsagar, S.W.; Patil, N.R.; Samant, S.D. One-Pot Synthesis of 2-Amino-5-Nitro-4,6-Diarylcyclohex-1-Ene-1,3,3-Tricarbo-Nitriles by Condensation of Aldehyde, Malononitrile, and Nitromethane in the Presence of Mg–Al HT under Solvent-Free Condition. *Tetrahedron Lett.* **2010**, *51*, 2924–2927. [CrossRef]
8. Surpur, M.P.; Kshirsagar, S.; Samant, S.D. Exploitation of the Catalytic Efficacy of Mg/Al Hydrotalcite for the Rapid Synthesis of 2-Aminochromene Derivatives Via a Multicomponent Strategy in the Presence of Microwaves. *Tetrahedron Lett.* **2009**, *50*, 719–722. [CrossRef]
9. Azarifar, D.; Tadayoni, M.; Ghaemi, M. γ-Fe_2O_3@Cu_3Al-LDH-TUD as a New Amphoteric, Highly Efficient and Recyclable Heterogeneous Catalyst for the Solvent-free Synthesis of Dihydropyrano[3,2-c]Pyrazoles and Dihydropyrano[3,2-c]Chromens. *Appl. Organomet. Chem.* **2018**, *32*, e4293. [CrossRef]
10. Reddy, T.N.; Ravinder, M.; Bikshapathi, R.; Sujitha, P.; Kumar, C.G.; Rao, V.J. Design, Synthesis, and Biological Evaluation of 4-H Pyran Derivatives as Antimicrobial and Anticancer Agents. *Med. Chem. Res.* **2017**, *26*, 2832–2844. [CrossRef]
11. Udhaya Kumar, C.; Pillai, M.V.; Gokula Krishnan, K.; Ramalingan, C. Synthesis, Experimental and Theoretical Studies on Highly Functionalized Novel 4H-Pyran-3-Carboxylate. *J. Mol. Struct.* **2019**, *1175*, 587–592. [CrossRef]
12. Aytemir, M.D.; Çaliş, Ü.; Özalp, M. Synthesis and Evaluation of Anticonvulsant and Antimicrobial Activities of 3-Hydroxy-6-methyl-2-substituted 4H-Pyran-4-one Derivatives. *Arch. der Pharm.* **2004**, *337*, 281–288. [CrossRef] [PubMed]
13. Banerjee, S.; Horn, A.; Khatri, H.; Sereda, G. A Green One-Pot Multicomponent Synthesis of 4H-Pyrans and Polysubstituted Aniline Derivatives of Biological, Pharmacological, and Optical Applications Using Silica Nanoparticles as Reusable Catalyst. *Tetrahedron Lett.* **2011**, *52*, 1878–1881. [CrossRef]
14. Kshirsagar, S.W.; Patil, N.R.; Samant, S.D. Mg-Al Hydrotalcite as a First Heterogeneous Basic Catalyst for the Synthesis of 4H-Pyrano[2,3-c]pyrazoles Through a Four-Component Reaction. *Synth. Commun.* **2011**, *41*, 1320–1325. [CrossRef]
15. Seshu Babu, N.; Pasha, N.; Venkateswara Rao, K.T.; Sai Prasad, P.S.; Lingaiah, N. A Heterogeneous Strong Basic Mg/La Mixed Oxide Catalyst for Efficient Synthesis of Polyfunctionalized Pyrans. *Tetrahedron Lett.* **2008**, *49*, 2730–2733. [CrossRef]
16. Zhang, X.; Yang, C.; Zhang, Y.; Xu, Y.; Shang, S.; Yin, Y. Ni–Co Catalyst Derived from Layered Double Hydroxides for Dry Reforming of Methane. *Int. J. Hydrogen Energy* **2015**, *40*, 16115–16126. [CrossRef]
17. van Dijk, H.A.J.; Walspurger, S.; Cobden, P.D.; van den Brink, R.W.; de Vos, F.G. Testing of hydrotalcite-Based Sorbents for CO_2 and H2S Capture for Use in Sorption Enhanced Water Gas Shift. *Int. J. Greenh. Gas Control* **2011**, *5*, 505–511. [CrossRef]
18. Perez-Lopez, O.W.; Senger, A.; Marcilio, N.R.; Lansarin, M.A. Effect of Composition and Thermal Pretreatment on Properties of Ni–Mg–Al Catalysts for CO_2 Reforming of Methane. *Appl. Catal. A Gen.* **2006**, *303*, 234–244. [CrossRef]
19. Zhang, J.; Zhao, N.; Wei, W.; Sun, Y. Partial Oxidation of Methane Over Ni/Mg/Al/La Mixed Oxides Prepared from Layered Double Hydrotalcites. *Int. J. Hydrogen Energy* **2010**, *35*, 11776–11786. [CrossRef]
20. Kaneda, K.; Mizugaki, T. Design of High-Performance Heterogeneous Catalysts Using Hydrotalcite for Selective Organic Transformations. *Green Chem.* **2019**, *21*, 1361–1389. [CrossRef]
21. Zeng, Y.; Zhang, T.; Xu, Y.; Ye, T.; Wang, R.; Yang, Z.; Jia, Z.; Ju, S. Cu/Mg/Al Hydrotalcite-Like Hydroxide Catalysts for O-Phenylphenol Synthesis. *Appl. Clay Sci.* **2016**, *126*, 207–214. [CrossRef]
22. Wierzbicki, D.; Baran, R.; Dębek, R.; Motak, M.; Grzybek, T.; Gálvez, M.E.; Da Costa, P. The Influence of Nickel Content on the Performance of Hydrotalcite-Derived Catalysts in CO_2 Methanation Reaction. *Int. J. Hydrogen Energy* **2017**, *42*, 23548–23555. [CrossRef]
23. Dębek, R.; Zubek, K.; Motak, M.; Da Costa, P.; Grzybek, T. Effect of Nickel Incorporation into Hydrotalcite-Based Catalyst Systems for Dry Reforming of Methane. *Res. Chem. Intermed.* **2015**, *41*, 9485–9495. [CrossRef]

24. Liu, Q.; Wang, C.; Qu, W.; Wang, B.; Tian, Z.; Ma, H.; Xu, R. The Application of Zr Incorporated Zn-Al Dehydrated Hydrotalcites as Solid Base in Transesterification. *Catal. Today* **2014**, *234*, 161–166. [CrossRef]
25. Zhou, W.; Tao, Q.; Pan, J.; Liu, J.; Qian, J.; He, M.; Chen, Q. Effect of Basicity on the Catalytic Properties of Ni-Containing Hydrotalcites in the Aerobic Oxidation of Alcohol. *J. Mol. Catal. A Chem.* **2016**, *425*, 255–265. [CrossRef]
26. Rives, V. Characterisation of Layered Double Hydroxides and Their Decomposition Products. *Mater. Chem. Phys.* **2002**, *75*, 19–25. [CrossRef]
27. Dębek, R.; Motak, M.; Galvez, M.E.; Grzybek, T.; Da Costa, P. Promotion Effect of Zirconia on Mg(Ni,Al)O Mixed Oxides Derived from Hydrotalcites in CO_2 Methane Reforming. *Appl. Catal. B Environ.* **2018**, *223*, 36–46. [CrossRef]
28. Kawabata, T.; Shinozuka, Y.; Ohishi, Y.; Shishido, T.; Takaki, K.; Takehira, K. Nickel Containing Mg-Al Hydrotalcite-Type Anionic Clay Catalyst for the Oxidation of Alcohols with Molecular Oxygen. *J. Mol. Catal. A Chem.* **2005**, *236*, 206–215. [CrossRef]
29. Qi, Y.; Cheng, Z.; Zhou, Z. Steam Reforming of Methane over Ni Catalysts Prepared from Hydrotalcite-Type Precursors: Catalytic Activity and Reaction Kinetics. *Chin. J. Chem. Eng.* **2015**, *23*, 76–85. [CrossRef]
30. Seftel, E.M.; Popovici, E.; Mertens, M.; Van Tendeloo, G.; Cool, P.; Vansant, E.F. The Influence of the Cationic Ratio on the Incorporation of Ti4+ in the Brucite-Like Sheets of Layered Double Hydroxides. *Microporous Mesoporous Mater.* **2008**, *111*, 12–17. [CrossRef]
31. Navarro, R.M.; Guil-Lopez, R.; Fierro, J.L.G.; Mota, N.; Jiménez, S.; Pizarro, P.; Coronado, J.M.; Serrano, D.P. Catalytic Fast Pyrolysis of Biomass over Mg-Al Mixed Oxides Derived from Hydrotalcite-Like Precursors: Influence of Mg/Al Ratio. *J. Anal. Appl. Pyrolysis* **2018**, *134*, 362–370. [CrossRef]
32. Gomes, J.F.P.; Puna, J.F.B.; Gonçalves, L.M.; Bordado, J.C.M. Study on the Use of MgAl Hydrotalcites as Solid Heterogeneous Catalysts for Biodiesel Production. *Energy* **2011**, *36*, 6770–6778. [CrossRef]
33. Liu, Y.; Suzuki, K.; Hamakawa, S.; Hayakawa, T.; Murata, K.; Ishii, T.; Kumagai, M. Highly Active Methanol Decomposition Catalyst Derived from Pd-Hydrotalcite Dispersed on Mesoporous Silica. *Catal. Lett.* **2000**, *66*, 205. [CrossRef]
34. Chang, X.; Zhang, X.; Chen, N.; Wang, K.; Kang, L.; Liu, Z.-H. Oxidizing Synthesis of Ni^{2+}–Mn^{3+} Layered Double Hydroxide with Good Crystallinity. *Mater. Res. Bull.* **2011**, *46*, 1843–1847. [CrossRef]
35. Shekoohi, K.; Hosseini, F.S.; Haghighi, A.H.; Sahrayian, A. Synthesis of Some Mg/Co-Al Type Nano Hydrotalcites and Characterization. *MethodsX* **2017**, *4*, 86–94. [CrossRef]
36. Costa, D.G.; Rocha, A.B.; Diniz, R.; Souza, W.F.; Chiaro, S.S.X.; Leitão, A.A. Structural Model Proposition and Thermodynamic and Vibrational Analysis of Hydrotalcite-Like Compounds by DFT Calculations. *J. Phys. Chem. C* **2010**, *114*, 14133–14140. [CrossRef]
37. Kosova, N.V.; Devyatkina, E.T.; Kaichev, V.V. Mixed Layered Ni–Mn–Co Hydroxides: Crystal Structure, Electronic State of Ions, and Thermal Decomposition. *J. Power Sources* **2007**, *174*, 735–740. [CrossRef]
38. Nishimura, S.; Takagaki, A.; Ebitani, K. Characterization, synthesis and catalysis of hydrotalcite-related materials for highly efficient materials transformations. *Green Chem.* **2013**, *15*, 2026–2042. [CrossRef]
39. Faramawy, S.; Zaki, T.; Sakr, A.A.E.; Saber, O.; Aboul-Gheit, A.K.; Hassan, S.A. The Activity of Mg-Al Layered Double Hydroxides Intercalated with Nitrogen-Containing Anions Towards the Removal of Carbon Dioxide from Natural Gas. *J. Nat. Gas Sci. Eng.* **2018**, *54*, 72–82. [CrossRef]
40. Soares Dias, A.P.; Bernardo, J.; Felizardo, P.; Neiva Correia, M.J. Biodiesel Production over Thermal Activated Cerium Modified Mg-Al Hydrotalcites. *Energy* **2012**, *41*, 344–353. [CrossRef]
41. Azath, I.A.; Puthiaraj, P.; Pitchumani, K. One-Pot Multicomponent Solvent-Free Synthesis of 2-Amino-4H-benzo[b]pyrans Catalyzed by Per-6-amino-β-cyclodextrin. *ACS Sustain. Chem. Eng.* **2013**, *1*, 174–179. [CrossRef]
42. Khurana, J.M.; Chaudhary, A. Efficient and Green Synthesis of 4H-Pyrans and 4H-Pyrano[2,3-c] Pyrazoles Catalyzed by Task-Specific Ionic Liquid [bmim]OH under Solvent-Free Conditions. *Green Chem. Lett. Rev.* **2012**, *5*, 633–638. [CrossRef]
43. Tanaka, K.; Toda, F. Solvent-Free Organic Synthesis. *Chem. Rev.* **2000**, *100*, 1025–1074. [CrossRef] [PubMed]
44. Malviya, J.; Kala, S.; Sharma, L.K.; Singh, R.K.P. Efficient Three-Component One-Pot Synthesis of 4H-Pyrans. *Russ. J. Org. Chem.* **2019**, *55*, 686–693. [CrossRef]

45. Van Laar, F.M.P.R.; De Vos, D.E.; Pierard, F.; Kirsch-De Mesmaeker, A.; Fiermans, L.; Jacobs, P.A. Generation of Singlet Molecular Oxygen from H2O2 with Molybdate-Exchanged Layered Double Hydroxides: Effects of Catalyst Composition and Reaction Conditions. *J. Catal.* **2001**, *197*, 139–150. [CrossRef]
46. Nope, E.; Martínez, J.; Rojas, H.; Sathicq, Á.; Romanelli, G. Synthesis of Mesoporous Ca-MCM Catalysts and Their Use in Suitable Multicomponent Synthesis of Polyfunctionalized Pyrans. *Res. Chem. Intermed.* **2016**, *43*, 2103–2118. [CrossRef]
47. D'Alessandro, O.; Sathicq, Á.G.; Sambeth, J.E.; Thomas, H.J.; Romanelli, G.P. A Study of the Temperature Effect on Hantzsch Reaction Selectivity Using Mn and Ce Oxides under Solvent-Free Conditions. *Catal. Commun.* **2015**, *60*, 65–69. [CrossRef]
48. Haas, C.P.; Tallarek, U. Kinetics Studies on a Multicomponent Knoevenagel−Michael Domino Reaction by an Automated Flow Reactor. *Chem. Open* **2019**, *8*, 606–614. [CrossRef]
49. Gupta, R.; Ladage, S.; Ravishankar, L. Mg-Al Hydrotalcite Catalyzed Efficient One-Pot Synthesis of 4-H-Benzo [b] Pyrans, 2-Aryl Benzimidazole and 2-Aryl-4, 5-Dihydro-1H-Imidazole Derivatives. *Chemistry* **2015**, *1*, 5–9.
50. Mokhtar, M.; Saleh, T.S.; Basahel, S.N. Mg–Al Hydrotalcites as Efficient Catalysts for Aza-Michael Addition Reaction: A Green Protocol. *J. Mol. Catal. A Chem.* **2012**, *353–354*, 122–131. [CrossRef]
51. Pavel, O.D.; Tichit, D.; Marcu, I.-C. Acido-Basic and Catalytic Properties of Transition-Metal Containing Mg–Al Hydrotalcites and Their Corresponding Mixed Oxides. *Appl. Clay Sci.* **2012**, *61*, 52–58. [CrossRef]
52. Zhao, S.Z.; Yi, H.H.; Tang, X.L.; Kang, D.J.; Yu, Q.J.; Gao, F.Y.; Wang, J.G.; Huang, Y.H.; Yang, Z.Y. Mechanism of Activity Enhancement of the Ni Based Hydrotalcite-Derived Materials in Carbonyl Sulfide Removal. *Mater. Chem. Phys.* **2018**, *205*, 35–43. [CrossRef]
53. Wang, D.; Zhang, X.; Liu, C.; Cheng, T.; Wei, W.; Sun, Y. Transition Metal-Modified Mesoporous Mg-Al Mixed Oxides: Stable Base Catalysts for the Synthesis of Diethyl Carbonate from Ethyl Carbamate and Ethanol. *Appl. Catal. A Gen.* **2015**, *505*, 478–486. [CrossRef]
54. Mancipe, S.; Tzompantzi, F.; Rojas, H.; Gómez, R. Photocatalytic Degradation of Phenol Using MgAlSn Hydrotalcite-Like Compounds. *Appl. Clay Sci.* **2016**, *129*, 71–78. [CrossRef]
55. Prihod'ko, R.; Sychev, M.; Kolomitsyn, I.; Stobbelaar, P.J.; Hensen, E.J.M.; van Santen, R.A. Layered Double Hydroxides as Catalysts for Aromatic Nitrile Hydrolysis. *Microporous Mesoporous Mater.* **2002**, *56*, 241–255. [CrossRef]